Spectral and Wavefront Error Performance of WFIRST/AFTA Bandpass Filter Coating Prototypes

Manuel A. Quijada
NASA Goddard Space Flight Center, MS 551
8800 Greenbelt Rd.
Greenbelt, MD 20771
301-286-3544
manuel.a.quijada@nasa.gov

Laurie Seide
SGT, Goddard Corporate Park,
7515 Mission Dr., Suite 300
Seabrook, MD 20706

Bert A. Pasquale
NASA Goddard Space Flight Center, MS 551,
8800 Greenbelt Rd.
Greenbelt, MD 20771

Joseph C. McMann
Sierra Lobo Inc,
6301 Ivy Lane, Suite 620
Greenbelt, MD 20770

John G. Hagopian
John Hagopian Engineering,
Harwood, MD 20776

Margaret Z. Dominguez
NASA Goddard Space Flight Center, MS 551
8800 Greenbelt Rd.
Greenbelt, MD 20771

Qian Gong
NASA Goddard Space Flight Center, MS 550
8800 Greenbelt Rd.
Greenbelt, MD 20771

Catherine T. Marx
NASA Goddard Space Flight Center, MS 551
8800 Greenbelt Rd.
Greenbelt, MD 20771

Abstract*—The Cycle 5 design baseline for the Wide-Field Infrared Survey Telescope Astrophysics Focused Telescope Assets (WFIRST/AFTA) instrument includes a single wide-field channel (WFC) instrument for both imaging and slit-less spectroscopy. The only routinely moving part during scientific observations for this wide-field channel is the element wheel (EW) assembly. This filter-wheel assembly will have 8 positions that will be populated with 6 bandpass filters, a blank position, and a Grism that will consist of a three-element assembly to disperse the full field with an undeviated central wavelength for galaxy redshift surveys. All filter elements in the EW assembly will be made out of fused silica substrates (110 mm diameter) that will have the appropriate bandpass coatings according to the filter designations (Z087, Y106, J129, H158, F184, W149 and Grism). This paper presents and discusses the performance (including spectral transmission and reflected/transmitted wavefront error measurements) of a subset of bandpass filter coating prototypes that are based on the WFC instrument filter compliment. The bandpass coating prototypes that are tested in this effort correspond to the Z087, W149, and Grism filter elements. These filter coatings have been procured from three different vendors to assess the most challenging aspects in terms of the in-band throughput, out of band rejection (including the cut-on and cut-off slopes), and the impact the wavefront error distortions of these filter coatings will have on the imaging performance of the wide-field channel in the WFIRST/AFTA observatory.

TABLE OF CONTENTS

978-1-4673-7676-1/16/$31.00

1. INTRODUCTION

The Wide-Field Infrared Survey Telescope Astrophysics Focused Telescope Assets (WFIRST/AFTA) instrument, which is the top-ranked large space mission in the New Worlds, New Horizon (NWNH) Decadal Survey of Astronomy and Astrophysics [1] is envisioned to be the next-generation space telescope (beyond the James Webb Space Telescope) with the goals of settling essential questions in both dark-energy research and exoplanet detection. In addition, the WFIRST/AFTA mission will advance our knowledge of topics ranging from galaxy evolution to the study of objects within the Milky Way Galaxy and our solar system. The current Design Reference Mission (DRM) for WFIRST/AFTA features a 2.4 meter aperture primary mirror (T1) with an on-axis secondary mirror (T2). The telescope hardware is an existing 2.4 meter, obscured two-mirror telescope made available to NASA from another United States Government agency [2]. Repurposing modifications will include small refiguring of the T1 conic, radius and conic adjustments of T2. In addition, there will be a conversion to a three-mirror anastigmat (TMA) optical configuration to enable a wide-field-of-view instrument and replacement of hardware that was not provided to NASA. The main instrument is a wide-field multi-filter near-infrared (NIR) system with imaging and spectroscopy capabilities. In addition, a coronagraph instrument has been added to the payload for direct imaging of exoplanets and debris disks. The Wide-Field Instrument (WFI) includes two modules: a wide field channel (WFC) and an integral field unit (IFU) spectrograph channel. The WFC instrument includes three mirrors, two folds (F1 and F2) and a tertiary (M3) and a filter/grism element wheel, with 7 positions plus a blank, to provide an imaging mode covering 750−2,000 nm and a spectroscopy mode covering 1,350−1,950 nm [3]. The performance of the bandpass filters used in both the imaging and spectroscopy mode are crucial to the functionality and scientific goals of the WFIRST/AFTA mission.

As part of the pre-formulation phase activities of the

WFIRST/AFTA mission, a risk-reduction effort was established at the Goddard Space Flight Center (GSFC) to procure and characterize up to three bandpass filter coatings that are deemed the most challenging to fabricate and meet spectral bandpasses and tight wavefront error distortion requirements. Hence, the purpose of this paper is to report the results of these characterization activities. The first part of the paper presents spectral bandpass characterization. The second part presents results of the component-level wavefront error (WFE) distortions produced by the coating stacks that define the bandpasses for each of these filters. The paper also presents an analysis of the system-level changes in the wavefront error (ΔWFE) and focus shift (ΔFocus) that are induced by these bandpass coatings WFE distortions in the WFIRST/AFTA Imaging Mode (WIM) optical model.

Section 2 provides an overview of the WFC instrument and the filter bandpass specifications derived from the Cycle 5 design report [3]. These bandpass specifications are determined from the optical system design requirements, which in turn, are driven by the mission science requirements. Section 3 describes the experimental setups that were used to perform spectral as well as wavefront error characterizations. Section 4 presents the results of the in-band and out-band spectral performance, as well as reflected and transmitted wavefront error measurements and analysis. Section 4 also includes an analysis and a discussion of the impact the WFE distortions of these bandpass coatings will have on the WFC imaging performance. The conclusions of the paper are presented in Section 5, where we also discuss some of the "lessons learned" as part of this risk-reduction effort.

2. WIDE-FIELD CHANNEL INSTRUMENT

Overview

As mentioned earlier, the WFC includes three mirrors (two folds and a tertiary) and an element wheel (EW) to provide an imaging mode covering 750−2,000 nm and a spectroscopy mode covering 1,350−1,950 nm. The WFC focal plane uses 18 4k×4k pixel-array HgCdTe detectors with 10 μm pixels. The HgCdTe detectors are arranged in a 6×3 array, providing an active area of $(0.281^\circ)^2$. The only moving part in the WFC assembly is the EW that has 8 slots: 6 filters, a blank, and a Grism assembly that will be used for galaxy redshift survey. Table 1 shows the spectral specifications for the six filters and the Grism assembly. The filter compliment specified in Table 1 indicates the wide-field imaging channel will have gapless observational coverage in the 750−2,000 nm spectral range.

Of the filter list shown in Table 1, it was decided (as part of a risk-reduction effort) to procure and characterize the 3 filters with the most challenging bandpass specifications. The W149 and Grism bandpass coatings deemed the two top candidates due to the very wide bandwidth of the former and the steep slope requirement of the latter. Of the remaining filters with resolution R= 4 (where R is the ratio of the center wavelength to the bandpass width at the 50% points), vendors were asked which one would be the most difficult to make. A consensus was reached that Z087 would be the most challenging, since it is the one with the shortest center wavelength and a blocking requirements that extends out to 3,000 nm. Hence, the Z087 was selected as the third choice to be included in this risk-reduction effort. Although the actual flight versions of these filters will have a slight meniscus-shaped substrates, a decision was made to use flat substrates instead, but with the full-size instrument aperture (110 mm).

Table 1. **The wide-field channel element wheel filter list.**

Filter ID	Min. (nm)	Max. (nm)	Center (nm)	Width (nm)	Slope (%)	R
Z087	750	977	869	217	3	4
Y106	927	1,192	1,060	265	3	4
J129	1,131	1,454	1,293	323	3	4
H158	1,380	1,774	1577	394	3	4
F184	1,683	2,000	1,842	317	3	5.8
W149	927	2,000	1,485	1,030	3	1.4
Grism	1,350	1,950	1,650	600	0.3	2.8

The substrate flatness requirement was set at a relatively tight requirement of less than $\lambda/2$ (at 632.8 nm) peak-to-valley (PV) surface figure (SF). This requirement was set in order to distinguish any distortion that may be induced by the stresses of the dielectric coating stacks used to form the bandpass of each filter. The procedure that was established for the filter coating prototype procurement is described next. We first procured ten fused silica blanks (Corning 7980) that had the nominal dimensions of 110 mm (diameter) and 6 mm (thickness) which match the Cycle 5 WIM filter substrate design. This type of fused silica was chosen due to its relatively flat response in the spectral range of interest. Upon receiving these parts, we characterized the WFE distortions in all of these substrates to make sure none of them exceeded the specified reflected surface figure of $\lambda/2$ (PV) at 632.8 nm. We also sent a request for quotes to several coating vendors with the desired spectral bandpass specifications that would be applied to these substrates. The specifications and bandpass requirements of the three filters (W149, Grism, and Z087) that were sent to each vendor are shown in Table 1. In addition, the statement of work (SOW) had the following requirements:

(1) All bandpass filter specifications will be for operation at 170 K.
(2) The nominal angle of incidence (AOI) is 0°. However, vendor shall make the best effort to minimize changes in transmittance bandpass when going to a maximum AOI of 16°.
(3) The changes in the WFE distortions (peak-to-valley) due to the coatings shall be no larger than λ/20 (transmitted) and λ/2 (reflected) at $\lambda = 632.8$ nm.
(4) Variation in the filter transmittance over the specified bandpass shall be less than 1% over the filter clear aperture of 105 mm.

Of the five proposals we received, three vendors were selected to produce versions of the W149, Z087, and Grism coating prototypes. We proceeded to send each vendor three of the 110 mm substrates (after WFE measurements were performed) so that each will get coated with the three filter coating designs the vendors produced. We also asked each vendor to provide additional 25 mm and 20 mm coupons of the same type of Corning 7980 substrate that will serve as witnesses coatings for each of the three 110 mm bandpass coating prototypes. The next task was to fully characterize each coated substrate to verify whether they met the specifications as provided in the SOW to each vendor.

The next section will described the equipment used for the

characterization of these coated substrates. These tests were designed to provide a quantitative analysis of the measured transmittance (in-band and out-of-band) in the visible and near-infrared wavelength regions. Next section will also describe the instrumentation used to measure the reflected and transmitted WFE distortions on each of the 110 mm uncoated and coated substrates.

3. EXPERIMENTAL DETAILS

Spectral Measurement

The instruments used to perform transmittance measurements in a focused beam geometry were a Bruker IFS 125HR Fourier Transform Infrared (FTIR)spectrometer (f/6.5 beam), and a Perkin Elmer (PE) Lambda 950 grating spectrometer (f/7 beam). The Bruker FTIR is a fast-scan instrument whose principle of operation is similar to that of a Michelson interferometer. The two light sources used are a globar and tungsten lamp for coverage in the NIR and visible spectral regions respectively (500−5,000 nm). Two combinations of detectors and beamsplitters were used to cover this spectral range. The wavelength range of 1,000−5,000 nm utilized an InSb detector and a CaF_2 beamsplitter, whereas the 500−1,000 range was covered with a silicon diode detector and a visible quartz beamsplitter. The PE Lambda 950 is a double-beam grating monochromator, ratio-recording spectrometer that offers a spectral coverage in the UV/VIS/NIR ranges (200−2,500 nm). The light sources are a tungsten-halogen lamp for the NIR and VIS ranges, and a deuterium (D_2) lamp for the UV region. The detectors used in this instrument are a photomultiplier tube (PMT) for the UV-VIS and an InGaAs detector for the NIR.

Transmittance data for these filters, $T(\lambda)$, were collected with the Bruker FTIR in the in-band spectral region, while the PE Lambda 950 was used for measurements in the out-of-band ranges. The data were normalized by taking the ratio of the filter spectral transmission, at a 0° angle of incidence, relative to the transmission of an empty hole. The estimated transmittance uncertainties for each of these instruments are $\pm 0.5\%$ (Bruker) and 7-8 absorbance units (PE). The wavelength accuracy is estimated to be ± 0.25 nm or better for either spectrometers. It is worth pointing out the f/#'s for each of these instruments are a fairly close match to the actual f/8 value of the WFIRST/AFTA telescope.

The temperature-dependent transmittance measurements in the visible/NIR spectral ranges were performed with the Bruker IFS 125HR equipped with a cryostat system described below. The temperature range of 100−300 K was possible by mounting the 25 mm coupons (one at a time) in a sample holder attached at the tip of an Oxford Instruments Optistat CF continuous flow cryostat. A flexible transfer line was used to flow liquid helium from a storage tank to the cryostat. The temperature of the sample was stabilized by using a temperature controller connected to a previously calibrated silicon diode sensor and heating element attached to the tip of the cryostat. In this setup, the temperature of the filter sample could be lowered by increasing the flow of liquid helium or raised by applying a current to the heater element. During measurements, the sample holder and cryostat units were placed inside a shroud equipped with optical windows in the spectrometer sample compartment. The pressure inside this shroud was kept below 10^{-6} Torr to prevent the formation of ice inside the cryostat or on the filter surface.

Wavefront Error Measurements

This section describes the procedure used to characterize the surface figure error of the 110 mm prototype bandpass coatings. Optical performance verification involved a multi-step process beginning with interferometric figure testing of the of the uncoated or blank substrates. Interferometric figure testing for the coated substrate was performed under several test conditions using visible and infrared Zygo interferometers. Visible wavelength interferometry was used to collect reflected surface figure errors since the source was at a He-Ne wavelength and due to the limited bandpass of the filter coatings for each of the three coating prescriptions. Infrared wavelength interferometry yielded surface figure errors plus transmitted wavefront errors for two of the three coating prescriptions (W149 and Grism) operating in the NIR region. Interferometric testing was performed in the following configurations:

(1) On the uncoated substrate at ambient room temperature using visible (632.8 nm) wavelength
(2) After coating at ambient room temperature using visible (632.8 nm) wavelength
(3) At cryogenic temperature of 160 K using visible (632.8nm) wavelength
(4) At room temperature using an interferometer with an infrared source centered at 1,550 nm wavelength.

The second and third configurations above utilized all of the as-delivered 110 mm coated samples, three from each "A" and "B" vendors plus two coated samples (Z087 and Grism) from vendor "C", since this vendor had not delivered their version of the W149 filter coating at the time of testing. The fourth configuration utilized two of the filter coatings whose bandpasses allowed for transmission of light at 1,550 nm. These are the W149 and the Grism samples from all three coating vendors. The first and second configurations were used to measure the bare substrate and coated sample at ambient temperature. This means that the same mount and interferometric test setup were used for these two configurations as shown in Fig. 1. An adapter assembly ring was fabricated to mount each of the 110 mm optics into a standard 6-inch Zygo tip-tilt mount as shown in the middle view of Fig. 1. The ring has two inner diameters. The larger inner diameter of 110.1 mm is slightly larger than the substrate and it was intended to evenly support the weight of the optic. The smaller inner diameter (108.5 mm) provides a reference surface against which to set the optic. The optic is retained inside the adapter between three # 8 screws with delrin washers on one side and Kapton tape "pads" affixed to the edge of the smaller inner diameter on the other side. Retaining screws were tightened until the slightest resistance was observed and then backed off to 1/4-turn to prevent optic distortion. The substrate in its mount was placed in front of the Zygo Mark-IV Interferometer as illustrated in the right view of Fig. 1. An edge mark indicated the "up" and front surface "S1" direction of the sample which was rotated visually into approximate location. Three or more data sets were recorded for "S1". The sample was then reversed so that the interferometer beam will impinge first on the second "S2" surface. Three or more additional data sets were recorded for this second surface.

The third configuration shown on the left-side image of Fig 2, illustrates the fact that measurements of the filter coatings at cryogenic temperature used a different mount and interferometric test setup. The right side of Fig. 2 shows how the sample was placed against a mounting plate on top of two pins wrapped with Kapton tape. The edge mark was

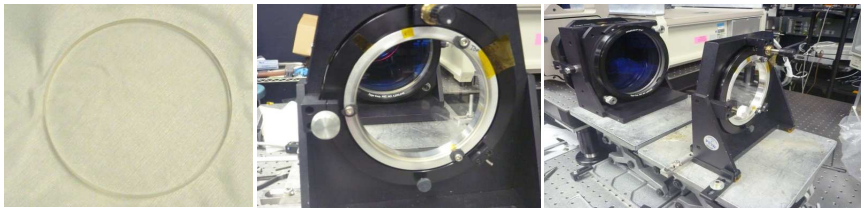

Figure 1. Left: Photo of substrate blank after unpacking. Middle: A substrate disk is shown mounted in the aluminum adapter ring which was rotated 30° clockwise for testing. Right: Surface measurement test setup with substrate mounted in Zygo tip/tilt assembly and reference flat attached to 4-to-6-inch beam expander on interferometer.

Figure 2. Left: The setup showing interferometer (left) and cryostat (right) for performing interferometric measurements at cryogenic temperatures. Right: Filter mounting scheme inside cryostat shown on left image.

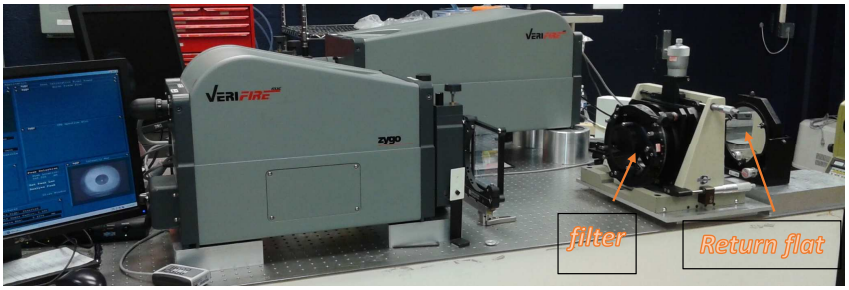

Figure 3. Transmitted wavefront error measurements setup showing an infrared interferometer (1,550 nm) and filter sample in a double pass configuration. A fold flat mirror is shown on the right side of the image behind the test filter mount.

positioned as before and the sample was secured on the top edge using Kapton tape. The sample holder assembly was placed inside the vacuum chamber shown on the left-side image. The procedure was to seal and pump down the chamber before the temperature of the test filter was cooled down to to 160 K using liquid nitrogen. Two or more data sets were recorded at temperature for "S1". After completion of "S1" measurements the chamber was warmed to room temperature and opened, and the process was repeated for the "S2" surface. The fourth configuration is illustrated in Fig. 3. This figure show the filter sample in front of an infrared Zygo interferometer, with a fold flat mirror behind to enable measurements of the transmitted wavefront in a double pass configuration. The test filter was mounted on a sample holder with a spring-loaded self-centering mount. The edge mark was positioned as before and the interferometer was calibrated per Zygo instructions. A single data set included the transmitted wavefront going through surfaces "S1" and "S2" plus a second pass of the transmitted wavefront error reflected off the fold mirror.

4. RESULTS

In-Band Spectral Performance

This section describes the spectral characterizations of the filter samples that were done with the spectrometers described in Sec. 3. We used the 25 mm coupons for these measurements which are witnesses to the large 110 mm optics given that it was only possible to measure these smaller samples using the cryostat available for these measurements. Figure 4 displays the transmittance in the 600−2,200 nm range at 170 K for the Grism, W149 and Z087 filters. This figure is a composite that illustrates the comparison of the filter sample performance from all three vendors. A qualitative comparison of Fig. 4 offers some worthwhile observations: The Z087 filter sample from vendor A exhibits some ripple in the in-band region while the versions of W149 and Grism for this vendor look much more smoother. This performance is in contrast to the results from vendor B, where the Z087 version appears much smoother, while the other two test filters from this vendor do exhibit more ripple (specially W149). Moreover, the results for the W149 filter coating prototype from vendor C did not meet the minimum in-band average transmittance of 95%. We performed a more quantitative analysis of these filter samples transmittance in the following way. For each of these curves, we calculated the

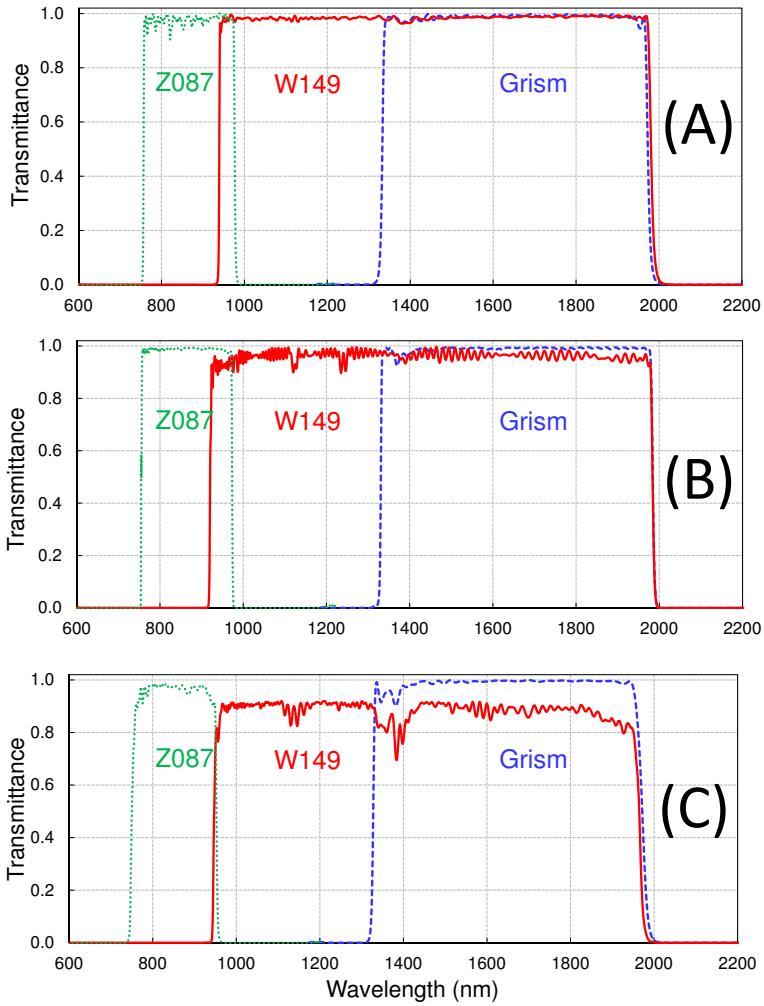

Figure 4. The transmittance of the 3 filter samples provided by three different vendors identified as A (top), B (middle), and C (bottom) at 170 K.

average in-band average transmittance (T_{ave}) by evaluating the formula:

$$T_{ave} = \frac{\int_{\lambda_{low}}^{\lambda_{high}} T(\lambda) d\lambda}{\lambda_{high} - \lambda_{low}}, \quad (1)$$

where $T(\lambda)$ is a function that represents the measured transmittance at a given wavelength λ. The λ_{low} and λ_{high} limits are the lower and upper wavelengths at which $T(\lambda) = 0.5 \cdot T_{ave}$. Notice that the limits in Eq. 1 are implicitly dependent on T_{ave}. Hence, a self-consisting solution to Eq. 1 is implemented by first using an initial guess of T_{ave} (based on the observed average transmission) and deriving the limits that are used in evaluating the integral in Eq. 1). Computation of the integral equation is complete when the computed T_{ave}, λ_{low} and λ_{high} parameters offer a self-consistent solution to Eq. 1. If not, the new λ_{low} and λ_{high} limits are derived from the newly determined T_{ave} and the integration is repeated until a self-consistent solution is satisfied.

Once this self-consistent solution is found, the slope or the rate of transmission increase at λ_{low} and λ_{high} are readily obtained from:

$$Slope = \frac{|\lambda_{0.9 \cdot T_{ave}} - \lambda_{0.1 \cdot T_{ave}}|}{\lambda_{0.5 \cdot T_{ave}}}, \quad (2)$$

where $\lambda_{0.9 \cdot T_{ave}}$, $\lambda_{0.1 \cdot T_{ave}}$, and $\lambda_{0.5 \cdot T_{ave}}$ are the wavelengths at which the transmittance values are 90%, 10%, and 50% of T_{ave} respectively.

Table 2 displays a quantitative analysis performed on the prototype Grism coatings for the three vendors that were derived from data shown in Fig. 4 and Equations 1 and 2. The numbers shown in green indicate the vendors met the required specification, whereas the numbers printed in red indicate indicate the filter coating prototype did not meet the given wavelength (within plus or minus the given tolerance). The numbers in yellow are meant to convey the fact that the filter sample came marginally close at meeting the requirement. The salient point in the results shown in Table 2 is that the vendors missed the tight slope requirement of 0.30% for the Grism coatings. The vendor that came closer to meeting the slope requirement (as defined in Eq. 2) is vendor B. The slope value in this case is roughly 25% larger than the target value (0.40% *versus* 0.30%). Otherwise, all vendors met the λ_{low} and λ_{high} parameters (with the exception of the λ_{high} for vendors A and C that came within $2-3$ nm respectively). All vendors exceeded the average in-band transmission by 4% (99% *versus* 95%). Finally, the temperature dependence is very modest with a shift in the λ_{low} and λ_{high} wavelengths in the order of $1-2$ nm. Table 3 shows the results of the

Table 2. Spectral bandpass parameters of Grism filter samples from three different vendors at 170 (data in parenthesis are at 295 K).

Grism	λ_{low} (nm)	λ_{high} (nm)	λ_{center} (nm)	T_{ave} (%)	Slope$_{low}$ (%)	Slope$_{high}$ (%)
Specs.	1,330 $\pm$5	1,980 $\pm$5	1,655 $\pm$5	$>$ 95	$<$ 0.30	$<$ 0.30
A	1,332 (1,333)	1,973 (1,975)	1,652 (1,654)	99	0.77	0.70
B	1,331 (1,332)	1,984 (1,986)	1,657 (1,658)	99	0.40	0.47
C	1,328 (1,329)	1,972 (1,974)	1,650 (1,652)	99	0.73	1.21

Table 3. Spectral bandpass parameters of W149 filter samples from three different vendors at 170 (data in parenthesis are at 295 K).

W149	λ_{low} (nm)	λ_{high} (nm)	λ_{center} (nm)	T_{ave} (%)	Slope$_{low}$ (%)	Slope$_{high}$ (%)
Specs.	925 $\pm$20	2,000 $\pm$20	1,465 $\pm$20	$>$ 95	$<$ 3	$<$ 3
A	940 (940)	1,981 (1,983)	1,460 (1,462)	98	0.42	0.77
B	920 (921)	1,984 (1,985)	1,452 (1,453)	98	0.93	0.45
C	945	1,965	1,452 (1,453)	88	1.15	1.83

Table 4. Spectral bandpass parameters of Z087 filter samples from three different vendors at 170 K (data in parenthesis are at 295 K).

Z087	λ_{low} (nm)	λ_{high} (nm)	λ_{center} (nm)	T_{ave} (%)	Slope$_{low}$ (%)	Slope$_{high}$ (%)
Specs.	758 $\pm$10	978 $\pm$10	868 $\pm$10	$>$95	$<$ 3	$<$ 3
A	757 (757)	976 (977)	866 (867)	97	0.54	0.58
B	755 (756)	973 (974)	864 (865)	99	0.51	0.42
C	750 (750)	952 (953)	851 (852)	95	1.57	0.61

analysis performed on all the W149 filter data. The sample from vendor C did not meet the λ_{high} and T_{ave} parameters. A second noteworthy observation is that the measured slopes for all three versions of the W149 filter coating are much tighter than the requirement of 3%. This tighter than required slope is a by-product of the requirement that filter bandpass coatings meet the out-of-band rejection requirements that will be discussed later in Sec. 4. Table 4 shows the tabulated spectral performance for the Z087 prototype coatings. This is another example where the test filter provided by vendor C did not meet the λ_{high} and λ_{center}. Otherwise, the other two vendors came within 3$-$4 nm in meeting the specified λ_{low} and λ_{high} wavelengths since the tolerance was set at $\pm$10 nm for this particular filter coating. The average in-band transmission exceeds the requirement: 97% and 99% *versus* 95% for vendors A and B respectively. The filter sample from vendor C met the T_{ave} at exactly 95 %. In regard to the measured slopes, we also observe they are much smaller than the requirement. As mentioned above, this is similar to the results on the W149 test filters and it is driven by the out-of-band blocking requirements.

Out-of-Band Rejection

Figure 5 shows these filter sample optical density (OD) over the 500$-$3,000 nm range, defined as OD = -log($T(\lambda)$, where $T(\lambda)$ is the measured wavelength-dependent transmittance (scaled from 0 to 1). Notice that the better a filter coating is at blocking out-of-band wavelengths, the higher the OD is in those wavelength regions. All these bandpass filters have an out-of-band rejection requirements that depend upon the specific filter bandpass regions. We observe that in the short or "blue" side (500$-$1,250 nm) of the Grism in-band region, the results yielded an average OD $>$ 4, while in the long or "red" side (2,050$-$2,500 nm) the OD $>$ 5. There is a region around $\lambda \approx 2,630$ nm, where the OD falls down to around 1$-$2, before it recovers to an average value of 3 up to 3,000 nm. It is interesting to note the data shown in Fig. 5 shows this behavior happened for both versions of Grism filters from vendors A and B (but not C). This dip in the filter OD performance at 2,630 nm will have to be addressed in a future flight version remake, depending if the detector quantum efficiency (QE) is significant beyond the longest observational wavelength of 2,000 nm in the WFC instrument. Otherwise, the performance shown for all three versions of the Grism coatings in Fig. 5 looks promising for the Grism filter prototype meeting its out-of-band rejection performance beyond the in-band spectral range.

We now discuss the OD performance data for the W149 filter sample shown in the middle panel of Fig. 5. In the region between 500$-$900 nm the OD is required to be around 4, while in the 2,050$-$3,000 nm range the OD is required to be larger than 5. While the results in Fig. 5 show the OD requirements of the W149 filter sample are met on the short side of the passband, the long side is only met up to 2,500 nm. The average OD values fall down to 4 up to 2,850 nm. It is not known yet if this OD performance will be adequate, given that the real QE performance will only be known after procurement and testing of these detectors is done as

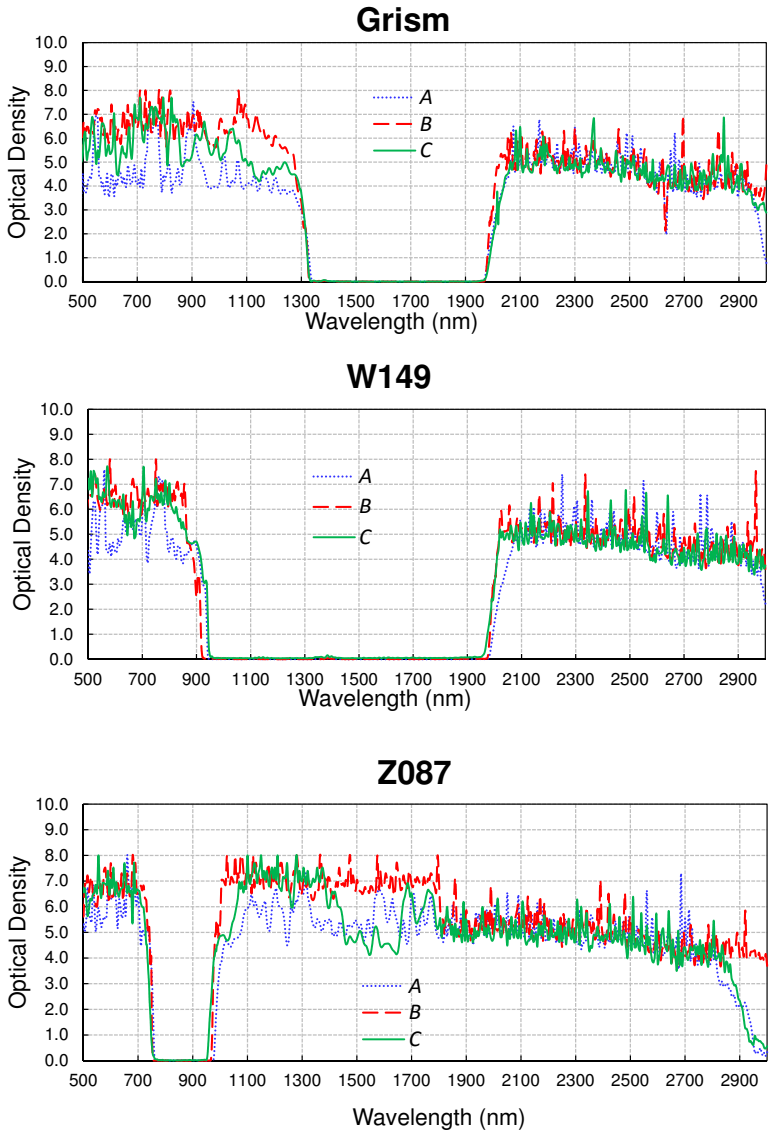

Figure 5. Comparison of Optical Density for the three filter samples from different vendors.

the WFIRST/AFTA mission moves later into formulation or flight status. We now discuss the OD results for Z087 that are shown at the bottom panel of Fig. 5. This particular filter has the following OD requirements: OD > 4 in the $500-740$ nm, while the OD is specified to be larger than 5 from 1,000 nm up to 3,000 nm. The three versions of the Z087 filter samples shown in Fig. 5 easily meet the OD requirement at least in the short or blue side of the in-band region. The OD performance at wavelengths longer than 1,000 nm varies from an observed average value of 5 up to 2,500 nm, and dropping to OD $\approx$ 4 (at least for vendor B) up to 3,000 nm. The performance for the Z087 produced by vendors A and C reached an OD of 4 only up to 2,800 nm, while these filter prototypes became somewhat transmissive above this wavelength.

Surface Figure Measurements Analysis

This section discusses interferometric surface figure error measurements that were performed on the large (110 mm) filter coating prototypes. These surface figure tests are critical because the high number of dielectric layers that are required to produce the desired bandpass is likely to cause surface stresses that, in turn, will degrade the coated surface figures. This degradation in figure will negatively impact the imaging performance of the WFC instrument. The vendors we contacted about procuring these coatings informed us that they have developed techniques to minimize the stress-induced distortion of the coatings on the substrate. However, they also advised us that it will be nearly impossible to ensure that the applied coating will not introduce any distortion on the substrate on which the coating stack is applied. In addition to WFE degradation, these distortions may also cause focus shift (in the case the optical coatings causes a "bowing" or curvature on the substrate after coating application). The specific types of aberrations that could be introduced are dependent on the nature of distortion caused by the applied coatings on the substrates. Therefore, it is paramount to measure the WFE distortion of the coated parts that will allow us to determine the impact these would have on the WFIRST/AFTA observatory imaging capability. Hence, these measurements are an important part of this risk-reduction effort.

The procedure we used to determine changes in the substrates

Table 5. . The RMS surface error in units of nanometers (nm) for uncoated and coated substrates. The numbers in the "Power" column that are derived from the interferometric data are also in units of nm. All measurements were done at ambient temperature (295 K), unless noted otherwise.

Vendor A

Filter ID	Side #	Uncoated RMS Surface	Uncoated Power	Coated RMS Surface	Coated Power	Coated RMS (160 K) Surface	Coated (160 K) Power
Grism	Side 1	69	227	529	-1,879	397	1,279
	Side 2	58	111	496	1,712	309	1,062
W149	Side 1	59	118	880	-3,037	509	-1,723
	Side 2	28	51	854	2,952	409	1,373
Z087	Side 1	53	49	2,026	7,020	1,538	5,327
	Side 2	90	182	1,856	-6,481	1,440	-4,998

WFE distortions after they were coated is described In Sec. 3. We first measured the surface figure error on the 110 mm uncoated substrates and we verified the distortion was not larger than $\lambda/2$ (PV) at 632.8 nm (or less than $\lambda/10$ RMS). These substrates were sent to the vendors for the application of the bandpass coatings. Upon their return to us, these coated parts were again interferometrically characterized both at ambient (295 K) and the cryogenic temperature of 160 K. A summary of these measurements is shown in Table 5 for the three filter sample sets from vendor A.

These results show that, for the most part, the filter prototypes from vendor A exhibit significant changes in the RMS surface figure errors. The filter prototype most severely affected is the Z087 with a RMS figure $\approx 2,026$ nm (Side 1 at 295 K). This surface also shows a coating-induced change in power (or focus shift) close to 7,020 nm at the same temperature. The optics with the next to the largest change in surface figure distortion is W149 (RMS surface error ≈ 880 nm or power $\approx -3,037$ nm (at 295 K). The Grism filter prototype showed the least changes in RMS surface error values ≈ 309 nm, and power $\approx 1,062$ nm (Side 2 at 160 K).

Next, we show the results of interferometric measurements performed on filter prototypes from vendor B. These results are shown in Table 6. The response seen in these coatings, in terms of RMS surface distortion appears to be the smallest when compared to the coated substrates from the other two vendors. The RMS surface and power numbers shown in Table 6 for this vendor are only marginally larger when compared to the uncoated substrate data.

Finally, we show in Table 7 the surface figure error distortion results obtained on two of the filter protoypes from vendor C (Grism and Z087).

Reflected Surface Figure Measurements and System Impact

The next step in the process of optical performance verification of the surface figures in these filter coating prototypes involved manipulating the interferometric data into a format that could be implemented in the optical model of the WIM system. The initial data manipulation was performed using MetroPro software, later upgrading to MX software. Data from the bare substrates, coated substrates at ambient, and at cryogenic temperatures (160 K) were processed in the same manner. Each data collection was processed independently, *i.e.*, one of the data sets would be either surface "S1" or "S2" for a given filter sample at either ambient or 160 K.

The MX software was used to "load and average data" for each data collection, ranging from two to seven files averaged per set. A 1% "minimum valid" option was selected to minimize data dropout. Default settings were selected for the remaining options, and no surface apertures were applied before averaging. After averaging, the Mask Editor was used to apply a 105 mm Surface Mask centered on the averaged data. MX attributes were checked to verify that during data collection an Interferometric Scale Factor of 0.5 was applied to account for the double-pass test configuration. Piston and Tilt were removed and the resulting processed data were saved as a new *.DATX file. This process was repeated for each data set for uncoated, ambient, and cryogenic measurement configurations. The final step for data manipulation of the reflected surface figure test configurations was to open each new averaged data file and compare the Zernike fit and residual to the averaged data set. Most of the data sets included second-surface reflections due to the nature of the coating bandpass measured at visible wavelength. The Zernike fit effectively removed the second-surface interference to provide a reasonable measure of the surface error. Each data set was then saved as a 12th order, 37-term Fringe Zernike *.INT file for later application to the Code V WIM optical model file. The "S1" and "S2" data were saved as surface type SUR interferograms. Care was taken to include the aperture size in the recorded data.

Tables 8 and 9 shows the result of the analysis described above by using the interferometric data taken on the Z087 and Grism filter prototypes from vendors A, B, and C. Table 10 displays the results for two W149 test filters from vendors A and B (as noted earlier, the W149 sample from vendor C was not available at the time these measurements were performed). We computed the change in the WIM optical system WFE (ΔWFE) and the change in focus (ΔFocus) due to the coated surface distortions. We also computed the ΔWFE and ΔFocus on the WIM optical system after removing the effect of the substrate from the coated substrate data.

At face-value, the filter coatings that met the requirement of not exceeding a contribution of 18 nm or larger to the ΔWFE of the WIM optical model wavefront performance are the Z087 and Grism coatings (from vendor B), and W149 (vendors A and B).

One caveat to the filter maximum allowance to the WIM ΔWFE performance is that the filter wavefront quality spec-

Table 6. The RMS surface error in units of nanometers (nm) for uncoated and coated substrates. The numbers in the Power column that are derived from the interferometric data are also in units of nm. All measurements were done at ambient temperature (295 K), unless noted otherwise.

		Vendor B					
Filter ID	Side #	Uncoated RMS Surface	Uncoated Power	Coated RMS Surface	Coated Power	Coated RMS (160 K) Surface	Coated (160 K) Power
Grism	Side 1	196	623	66	-128	148	-511
	Side 2	51	141	200	634	95	206
W149	Side 1	116	243	103	-334	50	-165
	Side 2	168	553	50	63	289	-82
Z087	Side 1	102	259	134	-410	235	-601
	Side 2	56	-48	200	682	185	638

Table 7. The RMS surface error in units of nanometers (nm) for uncoated and coated substrates. The numbers in the Power column that are derived from the interferometric data are also in units of nm. All measurements were done at ambient temperature (295 K), unless noted otherwise.

		Vendor C					
Filter ID	Side #	Uncoated RMS Surface	Uncoated Power	Coated RMS Surface	Coated Power	Coated RMS (160 K) Surface	Coated (160 K) Power
Grism	Side 1	44	-7	377	1,158	353	1,210
	Side 2	58	-60	299	-1,011	447	-1,528
Z087	Side 1	118	316	1,101	-3,820	1,342	-5,035
	Side 2	59	155	1,322	4,575	1,700	5,870

Table 8. The system impact of the Z087 filter prototypes RMS surface error distortions on the WIM optical system. *Substrate data used were collected at 295 K.

Z087		A		B		C	
		ΔWFE (nm)	ΔFocus (μm)	ΔWFE (nm)	ΔFocus (μm)	ΔWFE (nm)	ΔFocus (μm)
295 K	Filter WFE	62	–	33	–	71	–
No Refocus	Substrate Removed	42	–	24	–	49	–
295 K	Filter WFE	24	113	14	60	35	115
Using Refocus	Substrate Removed	18	77	20	24	41	43
160 K	Filter WFE	80	–	67	–	91	–
No Refocus	Substrate Removed*	92	–	72	–	67	–
160 K	Filter Errors	67	72	68	-5	58	131
Using Refocus	Substrate Removed*	88	37	72	-41	58	59

ification is derived from the sensitivities generated using the overall WFIRST-AFTA telescope plus the WIM optical model. In the wide-field imaging mode, all sensitivities (fabrication, alignment and stabilities (both compensated and uncompensated) are included in the 18 nm error budget allocation mentioned above [4]. The sensitivity values of ΔWFE and ΔFocus shown in Tables 8, 9, and 10 are individually generated by evaluating the degradation of the WFE RMS across the entire WIM field.

We should point out that removing the substrate effects from the coated substrate surface figure measurements did not always represent a reduction to the WIM wavefront error performance. Both the ΔWFE and ΔFocus quantities sometimes increased or decreased when the bare substrate surface figure errors were removed, specifically for the cryogenic data at 160 K. Some of these inconsistencies may be explained by the fact that, due to time constraints, the substrate interferometric data were only collected at room-temperature (295 K). Hence, it is reasonable to assume that the substrate removal process may have an unaccounted systematic error since the substrate interferometric data were collected at

Table 9. **The system impact of the Grism filter prototypes RMS surface error distortions on the WIM optical system. *Substrate data used were collected at 295 K.**

Grism		A		B		C	
		ΔWFE (nm)	ΔFocus (μm)	ΔWFE (nm)	ΔFocus (μm)	ΔWFE (nm)	ΔFocus (μm)
295 K	Filter WFE	25	–	46	–	71	–
No Refocus	Substrate Removed	59	–	17	–	49	–
295 K	Filter WFE	19	-33	12	93	35	115
Using Refocus	Substrate Removed	35	-94	16	-46	41	43
160 K	Filter WFE	243	–	44	–	35	–
No Refocus	Substrate Removed*	215	–	106	–	37	–
160 K	Filter WFE	53	428	31	-64	28	-60
Using Refocus	Substrate Removed*	72	367	30	-202	32	-48

Table 10. **The system impact of the W149 filter prototypes RMS surface error distortions on the WIM optical system. *Substrate data used were collected at 295 K.**

W149		A		B	
		ΔWFE (nm)	ΔFocus (μm)	ΔWFE (nm)	ΔFocus (μm)
295 K	Filter Errors	8	–	22	–
No Refocus	No Substrate	25	–	120	–
295 K	Filter Errors	7	-20	8	-50
Using Refocus	No Substrate	21	-49	64	-191
160 K	Filter Errors	39	–	91	–
No Refocus	Substrate Removed*	45	–	150	–
160 K	Filter Errors	23	-67	89	-40
Using Refocus	Substrate Removed*	13	-96	117	-181

room temperature in a setup without a cryostat (shown in Fig 1), whereas the cold (160 K) coated substrate surface figure data were collected inside a cryostat (setup shown in Fig. 2). Although the effect of the windows in the cryostat to the cold surface figure measurements is estimated to be negligible, this was something that was not verified during the course of this investigation.

Transmitted Wavefront Error and System Impact

We also perform transmitted WFE measurements at room-temperature on two of the filter prototype sets (W149 and Grism) from each of the three vendors. These measurements correspond to the fourth test described in Sec. 3 and the setup shown in Fig. 3. The data analysis in this case were handled differently (with respect to the reflected WFE analysis discussed earlier) for two reasons. First, there was only a single data point collected per data set, so averaging was not needed. Second, the infrared interferometer had a smaller aperture than the visible interferometer so the applied aperture mask was changed accordingly.

Figure 6 displays the transmitted wavefront error analysis for the W149 filter samples, and the impact on the WIM optical model. The data set is organized with the first column having three rows identifying the filter coatings from their respective vendors: A, B, and C. Each of those rows displays a representative interferogram plot (second column), the calculated impact to the system WFE performance (in nm) before and after removing the power or focus term from the filter sample interferometric data (third and fourth columns respectively). The fifth column has the amount of focus adjustment (in μm) that will be required to compensate for the power term in the filter sample interferometric data. The results shown in Fig. 6 indicate that the W149 filter prototype from vendor B has the lowest impact to the system WFE performance. The ΔWFE value of 10 nm (with focus adjustment) is nearly half of the total budget allocation of 18 nm that was mentioned earlier at the WIM system-level optical model. It is worthwhile noting the filter prototype from vendor A did not show any improvement in the ΔWFE value even after compensating with a focus adjustment. This suggests the aberrations that contribute to this filter coating WFE distorting have an astigmatic contribution as opposed to a power or piston term.

Figure 7 displays the impact of the transmitted WFE data for the Grism coatings on the WIM optical system. These results show that the filter prototype ΔWFE contributions from vendors A and B are 21 and 22 nm respectively (after focus removal). Taken at face value, these values indicate

W149	Interferogram Scale: ± 0.1 Waves	WFE Delta (RMS)	WFE Delta (Focus Removed)	Focus Shift
vendor A	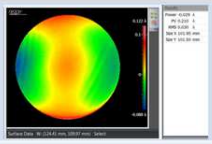	31 nm	31 nm	9 µm
vendor B	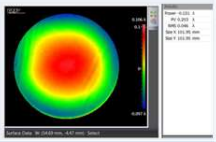	48 nm	10 nm	102 µm
vendor C	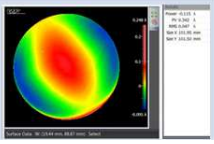	52 nm	44 nm	67 µm

Figure 6. **The system impact of the W149 filter prototypes transmitted RMS WFE distortions on the WIM optical system.**

Grism	Interferogram Scale: ± 0.1 Waves	WFE Delta (RMS)	WFE Delta (Focus Removed)	Focus Shift
vendor A	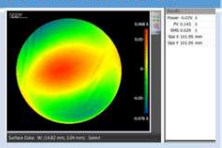	30 nm	21 nm	42 µm
vendor B	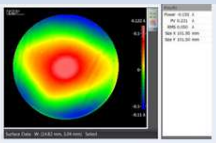	53 nm	22 nm	96 µm
vendor C	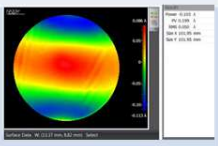	59 nm	46 nm	65 µm

Figure 7. **The system impact of the Grism filter prototypes transmitted RMS WFE distortions on the WIM optical system.**

that neither of these filter prototypes will meet the allocated ΔWFE contribution to the WIM optical model. Both filter prototypes are above the budgeted ΔWFE value of 18 nm by 3 and 4 nm for vendors A and B respectively. This means that more work will be required in a future flight procurement in order to ensure that the Grism and all the other filters in the WFC instrument will stay parfocal and meet the required WFE performance.

5. CONCLUSIONS

In conclusion, we characterized the spectral and wavefront error performance of a subset of three bandpass filter prototypes (Grism, W149, and Z087) that are defined in the filter complement of the Cycle 5 Design iteration for the WFIRST/AFTA wide-field channel instrument [3]. These bandpass filter prototypes were procured from three different coating vendors, in order to make a pre-selection of the vendor that will most likely meet the filter requirements in a future flight procurement. These filter prototypes were characterized by measuring and analyzing their optical transmittance in the $500-3{,}000$ nm range at room-temperature and 170 K. The W149 and Z087 filter prototypes from vendors A and B met key performance metrics such as average in-band transmission, the cut-on and cut-off wavelengths, slopes, and out-of-band rejections. Furthermore, none of the Grism coatings met all the spectral bandpass requirements. The Grism prototype coating from vendor B is the one that came closer in meeting the spectral requirements with the exception of the slopes on the on the low and high-side of the bandpass (slope $\approx$ 0.4% (measured) *versus* 0.3% (requirement). We also characterized the change in the WFE distortion of all the filter coatings by interferometrically measuring the WFE distortion performance on the substrate before and after application of the bandpass coatings. An analysis of these measurements suggested that the filter coatings from vendor B provided the least amount of WFE distortions and the smaller impact to the WFE of the WIM system optical model. A second analysis of the room-temperature transmitted WFE measurements performed on the W149 and Grism filter prototypes provided a qualitative confirmation that the samples from vendor B had the smallest WFE contribution to the WIM system optical model. This risk-reduction effort

provided some valuables lessons that will help in drafting specifications and requirements in a future procurement of the WFC flight filter bandpass coatings. Some of these lessons include increasing the substrate thickness from 6 mm to at least 8 mm in order to increase the substrate stiffness that could better withstand the stressed introduced by the coating stack. Secondly, every effort must be taken to characterize the bare substrate at the cryogenic temperature of operation prior to the coating application, in order to provide a better analysis of the coating impact to the total WFE budget of the WIM optical system. Finally, a wavelength tunable interferometric setup will have to be developed that will allow for testing the transmitted WFE distortion for all the filters at their respective bandpass wavelength ranges, since these measurements are likely to provide the most reliable WFE results in order to estimate the impact these bandpass coatings will have to the imaging performance of the WFIRST/AFTA observatory.

ACKNOWLEDGMENTS

We would like to acknowledge Kevin H. Miller (NASA-GSFC) for his assistance during spectral testing of the bandpass coating prototypes. We would also like to acknowledge Peter Morey (SGT) for assistance in performing the surface figure measurements on the large (110 mm) substrates before the bandpass coatings were applied. We are also grateful to Arthur Whipple (Conceptual Analytics, LLC) for his expertise in project management and for ensuring the various tasks performed under this risk-reduction effort were kept on a timely schedule.

REFERENCES

[1] Committee for a Decadal Survey of Astronomy and Astrophysics, [National Research Council, New Worlds, New Horizons in Astronomy and Astrophysics], The National Academies Press, Washington, D.C. (2010)

[2] Web site: http://www.space.com/21434-nasa-spy-satellite-telescope-wfirst.html

[3] Spergel, D.; Gehrels, N.; Baltay, C.; Bennett, D.; Breckinridge, J.; Donahue,M.; Dressler, A.; Gaudi, B. S.; Greene, T.; Guyon, O.; Hirata,C.; Kalirai, J.; Kasdin, N. J.; Macintosh, B.; Moos, W.; Perlmutter, S.; Postman, M.; Rauscher, B.; Rhodes, J.; Wang, Y.;Weinberg, D.; Benford, D.; Hudson, M.; Jeong, W. -S.; Mellier, Y.; Traub, W.; Yamada, T.; Capak, P.; Colbert, J.; Masters, D.; Penny, M.; Savransky, D.; Stern, D.; Zimmerman, N.; Barry, R.; Bartusek, L.; Carpenter, K.; Cheng, E.; Content, D.; Dekens, F.; Demers, R.; Grady, K.; Jackson, C.; Kuan, G.; Kruk, J.; Melton, M.; Nemati, B.; Parvin, B.; Poberezhskiy, I.; Peddie, C.; Ruffa, J.; Wallace, J. K.; Whipple, A.; Wollack, E.; Zhao, F.S. F. Gull, "Wide-Field InfraRed Survey Telescope-Astrophysics Focused Telescope Assets WFIRST-AFTA 2015 Report", 2015, oai:arXiv.org:1503.03757 [pdf]-**957085**

[4] Bert Pasquale, David Content, Jeffrey Kruk, David Vaughnn, Qian Gong, Joseph Howard, Alden Jurling, Len Seals, Eric Mentzell, Nerses Armani, Gary Kuan , "Optical Design of the WFIRST-AFTA Wide-Field Instrument"; Proc. SPIE 9293, International Optical Design Conference 2014, 929305 (December 17, 2014); doi:10.1117/12.2177847)

BIOGRAPHY

Manuel A. Quijada *received his B.S. and M.S. degrees in Physics from the University of Puerto Rico in 1987 and a Ph.D. in Solid State Physics form the University of Florida in 1994. He is currently a research physicist at the NASA Goddard Space Flight Center. His current research activities include the development of thin-film coatings for use in the far-ultraviolet spectral range.*

Laurie Seide *received her B.S. and M.S. degrees in Optical Sciences from the University of Arizona Optical Sciences Center in 1993 and 1995 respectively. She is currently a Senior Optical Analyst for Stinger Ghaffarian Technologies (SGT) in Greenbelt MD. She performs optical design, analysis, test, and verification of space-based optical instruments.*

Bert Pasquale *received his B.S. in Optics from the University of Rochester in 1991. He is currently an optical engineer and Optical Design Group leader at the NASA Goddard Space Flight Center. His current research activities include design and analysis for the Wide Field Infrared Survey Telescope - Astrophysics Focused Telescope Assets (WFIRST-AFTA).*

Catherine T. Marx *received her M.S. degree in Physics from the University of Maryland. She is a senior optical designer at the NASA Goddard Space Flight Center. She is currently the optics lead for WFIRST WFI.*

Margaret Z. Dominguez *received her B.S. in Physics from Universidad de las Americas Puebla (Mexico) in 2009, and her M.S. in Optical Sciences from the University of Arizona Optical Sciences Center in 2013. She is currently pursuing her Ph.D. at the University of Arizona while working as an optical engineer at the NASA Goddard Space Flight Center where she performs optical metrology, integration and testing.*

Dr. Qian Gong *received her Ph.D. from Optical Sciences Center, University of Arizona. She has been working on space optical systems and instruments since then. The instruments she has worked on cover the field of astrophysics, heliophysics, plenary science, and Earth science. The optical systems cover the imagers, spectrometers, Integral Field Spectrometer (IFS), Digital Micromirror Device (DMD), and coronagraphs. These instruments cover the wavelength range from UV to IR. Her current interest*

includes the slitless spectrometer for Wide-Field Infrared Survey Telescope (WFIRST), IFS for WFIRST coronagraph, and a DMD based UV spectrometer for Optical System for Galaxy Evolution Spectroscopic Explorer (GESE).

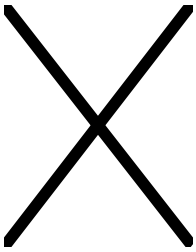

John G. Hagopian *received the BA in Astrophysics and MA in Nuclear Engineering from The University of Virginia. He was an Optical Physicist and Lead Engineer at the NASA Goddard Space Flight Center delivering instruments for the Cosmic Background Explorer, Broad Band X-Ray Telescope, Hubble Servicing Mission and Cassini Projects. These interferometer and imaging instruments span the electromagnetic spectrum. He served as ISIM, OTE and Mission Optical Systems Engineer on the James Webb Space Telescope for several years. He is currently working on ATALS and WFIRST in the role of Senior Alignment Integration and Test Optical Engineer for his company John Hagopian Engineering and has launched a startup company Advanced Nanophotonics, Inc., that is focused on commercialization of carbon nanotubes and other novel nanotechnologies.*